Earth Syst. Dynam., 3, 63–78, 2012
www.earth-syst-dynam.net/3/63/2012/
doi:10.5194/esd-3-63-2012
© Author(s) 2012. CC Attribution 3.0 License.

Earth System Dynamics

Solar irradiance reduction to counteract radiative forcing from a quadrupling of CO_2: climate responses simulated by four earth system models

H. Schmidt[1], K. Alterskjær[2], D. Bou Karam[3], O. Boucher[4,*], A. Jones[4], J. E. Kristjánsson[2], U. Niemeier[1], M. Schulz[5], A. Aaheim[6], F. Benduhn[7], M. Lawrence[7,], and C. Timmreck[1]**

[1]Max Planck Institute for Meteorology, Hamburg, Germany
[2]University of Oslo, Oslo, Norway
[3]Laboratoire des Sciences du Climat et l'Environnement, CEA, CNRS, UVSQ, Gif-sur-Yvette, France
[4]Met Office Hadley Centre, Exeter, UK
[5]Norwegian Meteorological Institute, Oslo, Norway
[6]Cicero, Oslo, Norway
[7]Max Planck Institute for Chemistry, Mainz, Germany
[*]now at: Laboratoire de Météorologie Dynamique, Institut Pierre Simon Laplace/CNRS, Paris, France
[**]now at: Institute for Advanced Sustainability Studies, Potsdam, Germany

Correspondence to: H. Schmidt (hauke.schmidt@zmaw.de)

Received: 13 January 2012 – Published in Earth Syst. Dynam. Discuss.: 25 January 2012
Revised: 8 May 2012 – Accepted: 14 May 2012 – Published: 6 June 2012

Abstract. In this study we compare the response of four state-of-the-art Earth system models to climate engineering under scenario G1 of two model intercomparison projects: GeoMIP (Geoengineering Model Intercomparison Project) and IMPLICC (EU project "Implications and risks of engineering solar radiation to limit climate change"). In G1, the radiative forcing from an instantaneous quadrupling of the CO_2 concentration, starting from the preindustrial level, is balanced by a reduction of the solar constant. Model responses to the two counteracting forcings in G1 are compared to the preindustrial climate in terms of global means and regional patterns and their robustness. While the global mean surface air temperature in G1 remains almost unchanged compared to the control simulation, the meridional temperature gradient is reduced in all models. Another robust response is the global reduction of precipitation with strong effects in particular over North and South America and northern Eurasia. In comparison to the climate response to a quadrupling of CO_2 alone, the temperature responses are small in experiment G1. Precipitation responses are, however, in many regions of comparable magnitude but globally of opposite sign.

1 Introduction

In the context of global warming, the study of climate engineering (CE, also known as "geoengineering") options has been proposed to prepare for the case that mitigation efforts fail or the consequences of the warming may prove more severe than expected. Over the last few years the number of scientific studies on the topic of CE in general, and on the CE option of solar radiation management (SRM) in particular has strongly increased. Additionally, a number of CE assessments have been published, aimed at the broader public and decision makers (e.g. Shepherd et al., 2009; GAO, 2011; Rickels et al., 2011).

SRM refers to artificial reduction in the amount of solar radiation reaching the surface of the Earth. Techniques suggested to reach this goal include mirrors in space (e.g. Mautner, 1991), injections of sulfur into the stratosphere to form particles and mimic the effect of large volcanic eruptions (e.g. Budyko, 1977; Crutzen, 2006), and the brightening of marine clouds by emissions of sea salt aerosols acting as cloud condensation nuclei (e.g. Latham, 1990). An overview of methods and an attempt to quantify their cooling potential is provided by Lenton and Vaughan (2009). Such

a deliberate global-scale manipulation of the radiative budget of the Earth may counterbalance the effects of continued greenhouse gas emissions on global surface temperature, but may also result in undesirable side effects for crucial parts of the Earth system and humankind. An SRM-engineered climate would regionally differ from a naturally balanced (say preindustrial) climate of the same global mean temperature because the local and temporal distribution of climate forcing from CE measures is different from the forcing caused by greenhouse gases (e.g. Govindasamy and Caldeira, 2000). But what would be the characteristics of such an engineered climate? Several studies have been performed with climate models in order to answer this question. Responses to different SRM methods show some robust characteristics, e.g. a decrease in global mean precipitation as discussed by Bala et al. (2008). However, in many details, for instance regional precipitation patterns, the responses differ across different models even if the same CE method is applied. It is unclear if the differences in climate response are related to the use of different models or different simulated scenarios. Several authors have therefore called for coordinated multi-model studies applying exactly the same scenarios (e.g. Jones et al., 2010; Irvine et al., 2010).

Kravitz et al. (2011b) proposed such a geoengineering model intercomparison study (GeoMIP) with a set of numerical experiments in which the climate forcing, as defined in experiments of the Climate Model Intercomparison Project 5 (CMIP5, Taylor et al., 2012), is balanced by SRM. Here we present an intercomparison of results for the G1 experiment of Kravitz et al. (2011b) performed by four different climate models of the ESM type, i.e. including full carbon cycles. Although the focus of GeoMIP is on the SRM method of sulfate aerosols, in G1 the top-of-atmosphere (TOA) forcing from an instantaneous quadrupling of the CO_2 concentration has to be balanced by a decrease of the solar constant (and thereby the total solar irradiance, TSI). This reduction of the solar constant may be considered as mimicking the effect of space mirrors, or simply as a generic approach to SRM. However, the experiment, utilizing an instantaneous quadrupling of CO_2, cannot be considered as a realistic scenario. The motivation for G1 is that it allows a model intercomparison using a simple way of implementing SRM in a climate model in an experiment where a high signal-to-noise ratio can be expected. This will facilitate the interpretation of future, potentially more realistic experiments, where sulfate CE is implemented in models in different ways (according to each model's capacity of treating stratospheric aerosols) to balance smaller forcings in transient 21st century scenarios. But it should also be noted that the magnitude of the forcing from quadrupling CO_2 is not completely out of the range of CMIP5 scenarios since a similar forcing would be reached around the end of the 21st century under the highest CMIP5 emission scenario RCP8.5 (Moss et al., 2010). The goal of this study is to assess to what extent climate change signals in the GeoMIP scenario G1, compared to a preindustrial control simulation, are robust or not, based on a set of four complex state-of-the-art Earth system models.

Experiments where either a doubling or quadrupling of CO_2 concentrations was balanced through a reduction of the solar constant have been performed earlier (e.g. Govindasamy and Caldeira, 2000; Govindasamy et al., 2003; Bala et al., 2008; Lunt et al., 2008; Irvine et al., 2010; Pongratz et al., 2012). In all experiments the reduction of the solar constant was such that the global mean temperature was approximately the same as in the period before the increase in CO_2 concentration and application of CE, but the globally-averaged precipitation rate decreased. A comparison of further quantities among the published studies is difficult because not all of them published the same parameters. Some differences among simulations were however mentioned. Irvine et al. (2010) report that they needed a solar constant reduction of 4.2 % to balance CO_2 quadrupling while in the experiment of Govindasamy et al. (2003) a reduction of 3.6 % was sufficient. In a simulation where transient greenhouse gas (GHG) forcing was balanced by a solar constant reduction, changing with time, Matthews and Caldeira (2007) studied regional responses. They found a precipitation decrease that is stronger over some continental regions than over the oceans and a decrease of the meridional temperature gradient. The latter is also evident from some of the above mentioned non-transient studies.

Results from specifically designed model intercomparison studies of CE experiments have not yet been published to our knowledge. Jones et al. (2010) compared responses of two climate models to sulfate aerosol CE in slightly different transient scenarios. Ricke et al. (2010) compared large ensembles of different transient SRM scenarios using a single, simple model in terms of regional responses. They concluded that despite similarities in global responses, the impacts may differ strongly regionally. Here we extend these previous studies by examining results from four models which carry out identical simulations.

Our manuscript is organized as follows. Section 2 describes the models used in this intercomparison and the GeoMIP G1 experiment. Section 3 provides a comparison of the amount of solar constant reduction necessary in the different models. The climate resulting from scenario G1 is compared to the preindustrial control climate in Sect. 4. To allow a comparison of signals resulting from CE with the simulated climate under non-balanced quadrupling of CO_2 most figures present responses obtained in the two scenarios side by side. However, unless relevant for understanding the response to G1, responses to quadrupling of CO_2 are discussed and compared to G1 only in Sect. 5. Section 6 deals with the response of the monsoon systems to G1. Section 7 provides a summary and conclusions.

Table 1. Main characteristics of the participating ESMs.

Name of the ESM reference	IPSL-CM5A Dufresne et al. (2012)	MPI-ESM Giorgetta et al. (2012)	NorESM Alterskjær et al. (2012)	HadGEM2-ES Collins et al. (2011)
Atmosphere model (resolution; lid) reference	LMDz (2.5° × 3.75°/L39; 65 km) Hourdin et al. (2011)	ECHAM6 (T63/L47; 0.01 hPa) Stevens et al. (2012)	CAM-Oslo (based on CAM4) (1.9° × 2.5°/L26; 2 hPa) Seland et al. (2008)	HADGEM2-A (1.25° × 1.875°/L38; 40 km) The HadGEM2 Development Team (2011)
Ocean model (resolution) reference	NEMO (96x95 gridpoints, L39) Madec (2008)	MPIOM (∼1.5°, L40) Marsland et al. (2003)	(based on) MICOM (∼1°, L70) Assmann et al. (2010)	HadGEM2-O (1/3 to 1°, L40) The HadGEM2 Development Team (2011)
Land/Vegetation model reference	ORCHIDEE Krinner et al. (2005)	JSBACH Raddatz et al. (2007)	CLM4 Oleson et al. (2010)	MOSES-II Essery et al. (2003)

"LXX": XX indicates the number of vertical layers; "TYY": triangular truncation at wavenumber YY.

2 Description of models and scenarios

Four different Earth system models (ESM) have been used in this study to perform the GeoMIP experiment G1 in which an instantaneous quadrupling of the CO_2 concentration is balanced by a decrease of solar irradiance represented by the solar constant and run for 50 yr. One reference experiment for G1 is the CMIP5 experiment 6.3 (Taylor et al., 2012, hereafter called abrupt4xCO2) which is started from the preindustrial control run (CMIP5 experiment 3.1; using a CO_2 volume mixing ratio of 285 ppmv), and runs for 150 yr after the quadrupling of CO_2 to 1139 ppmv. The second reference experiment is precisely this preindustrial control run continued from the same starting conditions as the G1 and abrupt4xCO2 experiments (hereafter called piControl).

The four climate models are the Met Office Hadley Centre ESM (HadGEM2-ES, Collins et al., 2011), the Institut Pierre Simon Laplace ESM (IPSL-CM5A, Dufresne et al., 2012), the Max Planck Institute ESM (MPI-ESM, Giorgetta et al., 2012), and the Norwegian ESM (NorESM, Alterskjær et al., 2012). The main characteristics of these models are given in Table 1. All models have been used for the simulation of a large number of experiments defined by the CMIP5 protocol. Results of these simulations are currently being used in numerous model intercomparison studies. Hence we will not evaluate the model performance with respect to preindustrial or present-day climate in this study. In Sect. 5 we will, however, compare some aspects of the simulated climates in the abrupt4xCO2 experiments, but mainly in order to allow a comparison of the geoengineered climate as in experiment G1 to a climate modified by a strong increase of CO_2 alone. We will also not discuss in detail the differences in the design of the four ESMs, and the reader is referred to the respective publications on the individual models. All models, however, are state-of-the-art coupled three-dimensional atmosphere-ocean-land surface models with deep ocean modules, generally well represented stratospheres, and interactive carbon cycles. Table 1 indicates that none of the models share major components (i.e. atmosphere, ocean and land/vegetation modules) and also the grid resolutions chosen in the model components differ. A priori this should increase the confidence in our findings when these are supported by results from all of the four models.

According to the G1 experiment specifications by Kravitz et al. (2011a) the forcing from the quadrupling of CO_2 (F_{4CO_2}, see Sect. 3) was balanced in each model by a reduction of the solar constant estimated as $\delta S_0 = -4\, F_{4CO_2}/(1-\alpha)$ to account for the sphericity of the Earth and the planetary albedo α. Then the experiment with increased CO_2 and reduced solar constant has been integrated for 10 yr and the 10-yr average net TOA radiative imbalance has been calculated. According to the GeoMIP specifications, the forcings can be considered as balanced if this average imbalance is below 0.1 W m^{-2}. If this is not the case the simulation has to be repeated with an adjusted δS_0 until the criterion is fulfilled. For all four models the necessary reduction of the solar constant had to be estimated in several iterative steps. Hence, the G1 experiments analyzed in this study, that span 50 yr of simulation time, all show a net TOA radiative imbalance below 0.1 W m^{-2} over the first 10 yr compared to piControl. No ensemble but only one single simulation has been performed with each of the four ESMs.

In Sects. 3 and 4 we compare the 50 yr of G1 with a 50-yr period of piControl that starts with the same initial conditions. All numbers and figures show differences between averages over these 50-yr periods. One may argue that an initial period should be left out from the averaging. However, global averages of major climate parameters show no discernible spin-up after the start of G1. Potential regional spin-up effects are accepted in order to increase the significance of the results using a long averaging period. Results presented in Sect. 5 use years 101 to 150 of the abrupt4xCO2 simulation in comparison to the same 50-year period of piControl described above. It should be noted that the abrupt4xCO2 simulations are still not in equilibrium at the end of the full 150 simulated years.

In the following, for many parameters only average responses of the four models are presented. In order to allow an estimation of the robustness of the responses, we indicate regions where all models agree in the sign of the response but

Table 2. Comparison of TOA forcings from quadrupling CO_2, total solar irradiance (TSI) reduction, and clouds.

	IPSL-CM5A	MPI-ESM	NorESM	HadGEM2-ES
Forcing from $4 \times CO_2$ ($W\,m^{-2}$)	6.4	9.6	7.5	6.8
TSI reduction in G1 ($W\,m^{-2}$)	48	64	55	53
(percentage)	(3.5 %)	(4.7 %)	(4.0 %)	(3.9 %)
Forcing from TSI reduction ($W\,m^{-2}$)	-8.4	-11.3	-9.6	-9.4
Efficacy of TSI reduction	0.76	0.85	0.78	0.72
SW cloud forcing (piControl) ($W\,m^{-2}$)	−53.3	−49.4	−54.3	−43.6
(G1-piControl, estimated) ($W\,m^{-2}$)	1.9	2.3	2.2	1.7
(G1-piControl, simulated) ($W\,m^{-2}$)	3.9	4.8	4.2	2.5

See text for further specifications.

do not consider statistical significances of the single model simulations.

3 Reduction of solar constant needed to balance a quadrupling of the CO_2 concentration

The forcing in the abrupt4xCO2 experiments has been estimated using the approach suggested by Gregory et al. (2004) where the regression of annual mean TOA net flux imbalances onto the corresponding globally-averaged near surface air temperature (SAT) anomalies is extrapolated to a value of $\Delta SAT = 0$. This method has been shown to provide reasonable forcing estimates in comparison to other methods (e.g. Hansen et al., 2005) and avoids extra simulations with a double radiation call. However, the forcing resulting from this method may include rapid feedbacks and has to be considered as an adjusted forcing (Gregory and Webb, 2008). Forcing estimates resulting for the four ESMs are given in the first line of Table 2. They range from $6.4\,W\,m^{-2}$ for the IPSL-CM5A to $9.6\,W\,m^{-2}$ for the MPI-ESM. The latter value seems high in comparison with the "best estimate" of radiative forcing due to CO_2 doubling of $3.7\,W\,m^{-2}$ (Ramaswamy et al., 2001), which would suggest forcing due to CO_2 quadrupling of $7.4\,W\,m^{-2}$. However, in the case of the MPI-ESM about $2\,W\,m^{-2}$ result from a rapid cloud feedback, the origin is not yet understood. Rapid feedbacks with different signs have also occurred in other climate models and been discussed by Gregory and Webb (2008).

From these forcing estimates, reductions of the solar constant necessary to balance the CO_2 forcing were estimated, as described in the previous section. However, in all four models larger reductions in TSI were necessary to reach a TOA balance below $0.1\,W\,m^{-2}$, as indicated by the values given in Table 2. The efficacy E_{TSI} (Hansen et al., 2005) of the solar forcing (F_{TSI}) with respect to forcing from CO_2 can be calculated from the ratios of the respective climate sensitivities:

$$E_{TSI} = \frac{\Delta T_{TSI}/F_{TSI}}{\Delta T_{4CO2}/F_{4CO2}}, \quad (1)$$

where the ΔT describes the SAT response to the respective forcing. Assuming the respective temperature responses for solar and CO_2 forcing in the balanced G1 experiment are equal (but of opposite sign), one can easily calculate the efficacies (see Table 2). Values for the four ESMs range between 0.72 and 0.85, with the highest value coming from the MPI-ESM and being influenced by the rapid cloud feedback mentioned above. Hansen et al. (2005) also calculated (with the GISS model III) that direct solar forcing is less effective than an equivalent CO_2 forcing. However, Hansen et al. (2005) report efficacies close to a value of 0.9 for solar constant reduction of similar magnitude to that in our simulations. In our case the low efficacies are at least partly related to a cloud response. Table 2 provides the shortwave (SW) cloud forcings in the four ESMs, i.e. the difference between net TOA SW radiation for the full model and for a calculation assuming clear-sky conditions. A reduction of the solar constant would lead to a reduction of the SW cloud forcing by the same percentage if clouds remained unchanged. The change in SW cloud forcing between G1 and piControl "estimated" under this assumption is provided in Table 2. The actually simulated change is, however, larger than this in all four ESMs, which can be explained by a smaller planetary albedo caused by reduced cloud cover in G1 compared to piControl (see also Sect. 4.5). Therefore a stronger than expected reduction of the solar constant is required. It is, however, clear that other processes than the SW cloud forcing contribute to the efficacies. HadGEM2-ES, for instance, has the lowest efficacy but the smallest SW effect of changed cloudiness ($0.8\,W\,m^{-2}$ difference between "expected" and simulated SW cloud forcing). Further studies will be necessary to better understand this effect. Changes in LW cloud forcing play a minor role. They are of opposite sign than changes in SW cloud forcing but of smaller magnitude in all four ESMs.

Figure 1 shows the multi-model and multi-annual mean geographical distribution of differences of TOA net downward fluxes between experiments G1 and piControl for the longwave (LW, terrestrial) and shortwave (SW, solar) radiation and for the total flux, i.e. the sum of both components.

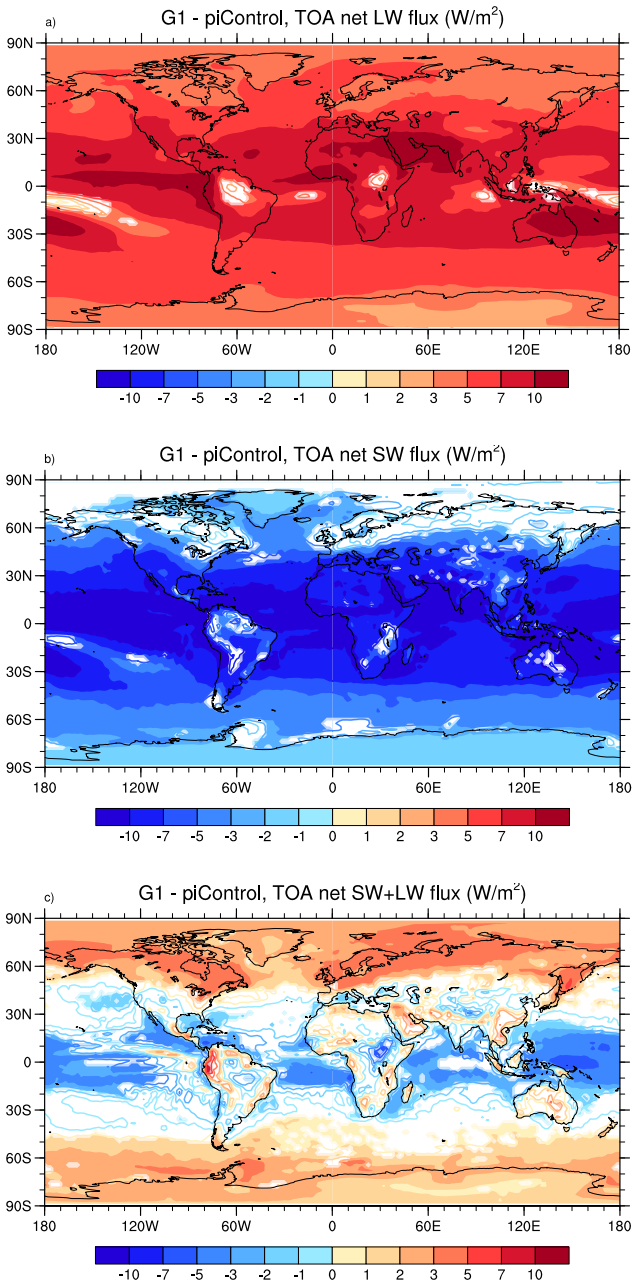

Fig. 1. Differences in TOA (top-of-atmosphere) net downward radiation fluxes between the simulations G1 and piControl in $W\,m^{-2}$, averaged over the four ESMs. Top panel: longwave (terrestrial), middle panel: shortwave (solar), bottom panel sum of long and short wave. In regions with filled color shading all models agree in the sign of the response. The value represented by the contours is given by the upper edge of the respective range in the color bar, i.e. the zero line is colored light blue.

The patterns largely reflect the forcings applied to G1, but of course also include feedback effects. The multi-model difference in LW radiation, mainly caused by the quadrupling of CO_2, is positive everywhere with the highest values in low latitudes, and only some models show small patches of negative differences in the tropics related to cloud feedbacks. The multi-model difference in SW radiation, mainly caused by the reduction of the solar irradiance, is negative everywhere with very high values of generally more than $10\,W\,m^{-2}$ in the tropics and less than $2\,W\,m^{-2}$ at polar latitudes. In particular, at high northern latitudes the models disagree in the sign of the response. In addition to clouds, sea ice and snow cover feedbacks influence the SW radiative balance at high latitudes. The globally-averaged total TOA flux imbalance is close to zero in all models over the 50 yr period (see Table 3), although not below $0.1\,W\,m^{-2}$ as required in G1 for the first 10 yr of the simulation. Regionally, this looks very different: the difference in total fluxes is in general weakly negative in the tropics and positive at high latitudes. This is mainly caused by the latitude dependence of the forcings, which is stronger for the solar constant reduction than for the increase of CO_2. Additionally, the seasonal cycles of TOA total fluxes differ between the experiments (not shown), because the effect of a reduction of the solar constant depends on the zenith angle at a specific location and time. These differences have already been pointed out by Govindasamy and Caldeira (2000) and are reasons why the climates simulated in G1 and piControl will differ despite a balanced globally-averaged TOA radiation. In the next section, we will describe the differences in the two simulated climates.

4 Differences between a geoengineered and preindustrial climate

4.1 Surface energy budget

Figure 2 shows the zonally-averaged multi-annual mean response of the surface energy budget to forcing in the G1 experiment for the four ESMs. All models respond similarly. The largest responses occur in the net surface SW flux and in the latent heat flux. The latitudinal dependence of the SW flux response is similar to the corresponding TOA response (Fig. 1) with maximum decreases (of about 6 to $9\,W\,m^{-2}$) in the tropics and much smaller signals at high latitudes. This decrease in downward energy flux is largely compensated by decreasing latent heat flux. All other components of the surface energy budget show much smaller absolute changes. The response of the LW flux is in general positive with globally-averaged values of about 1 to $2\,W\,m^{-2}$, a weak minimum close to the equator and weak local maxima in the subtropics. The total net downward energy flux also has a minimum at the equator (of values close to $-2\,W\,m^{-2}$) and weakly positive responses at most other latitudes. This implies a reduced energy transfer away from the equator in the oceans. Bala et al. (2008) have discussed the surface energy balance in a similar simulation (balancing of CO_2 doubling). They also describe that the weaker SW flux in the engineered climate is mainly balanced by a weaker latent heat flux. They

Table 3. Comparison of differences between the geoengineered and preindustrial climates (G1 – piControl) in globally-averaged parameters.

	IPSL-CM5A	MPI-ESM	NorESM	HadGEM2-ES
TOA net flux ($W\,m^{-2}$)	0.01	0.13	−0.02	0.15
SAT (K)	0.10	−0.03	−0.03	0.20
Precipitation ($mm\,day^{-1}$)	−0.16 (−6.1 %)	−0.11 (−3.6 %)	−0.14 (−5.0 %)	−0.13 (−4.2 %)
Cloud fraction	−0.010 (−1.7 %)	−0.010 (−1.6 %)	−0.006 (−1.1 %)	−0.008 (−1.5 %)
Planetary albedo	−0.008 (−2.5 %)	−0.009 (−2.6 %)	−0.006 (−1.8 %)	−0.008 (−2.6 %)

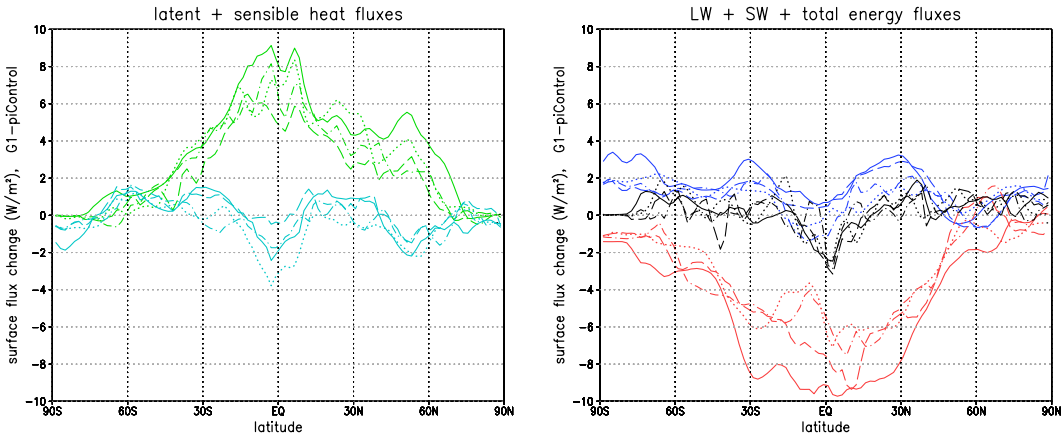

Fig. 2. Differences in zonally-averaged surface net downward energy fluxes between the simulations G1 and piControl in $W\,m^{-2}$ from the four ESMs. Solid: IPSL-CM5A, dashed: MPI-ESM, dotted: NorESM, dot-dashed: HadGEM2-ES. Left panel: latent (green) and sensible (cyan) heat fluxes; right panel: longwave radiation (blue), shortwave radiation (red) and sum of all four components (black). All fluxes are defined as positive in the downward direction.

explain this, citing Hansen et al. (1997), with the different hydrological sensitivities resulting from greenhouse gas and solar forcing as a result of solar forcing mainly heating the surface and CO_2 mainly heating the troposphere.

Figure 3a shows that the latent heat response depends strongly on the location. Vegetation covered land masses (South America, tropical Africa, South East Asia, North America, and Northern Eurasia) show in general a stronger decrease of the latent heat flux than oceans at the same latitude. This may be related to the response of stomatal conductance in plants to changes in the CO_2 concentration, an effect that is represented in all four ESMs. Under increased CO_2, this tends to reduce the evaporation from plants and hence the latent heat flux. This mechanism has also been proposed (e.g. Joshi and Gregory, 2008) to contribute to the land-sea contrast in the surface temperature increase caused by greenhouse gases (Fig. 3d). Accordingly, similar differences between latent heat flux changes over land and ocean are also simulated by the four ESMs as a response to quadrupling of CO_2 (Fig. 3b). The reduced latent heat flux also contributes to and is influenced by the reduction of precipitation (as discussed in Sect. 4.4).

4.2 Surface air temperature

The responses of globally-averaged near surface air temperature (SAT) to the forcing in G1 are small (Table 3), as can be expected as a result from a globally-averaged TOA radiative forcing close to zero. SAT changes range from −0.03 K in MPI-ESM and NorESM to 0.2 K in HadGEM2-ES. The dependence of the SAT response on latitude is similar in all four ESMs (Fig. 4a). All models indicate a weak cooling (up to −0.5 K in the MPI-ESM) in zonally-averaged tropical SAT, and a warming in high latitudes. While Antarctic SAT increases on average by about 0.6 K with small differences between the models, the temperature increase in the Arctic ranges from about 0.8 K (NorESM) to 1.8 K (HadGEM2-ES). Different ice and cloud albedo feedbacks are responsible for the variability of the responses in this region. It should be noted that multi-decadal variability in some of the ESMs is strong in the North-Atlantic region, so that differences between the single models from a comparison of 50-yr averages may not be statistically significant in all cases. The reduction of the meridional temperature gradient visible in all models has also been simulated earlier, e.g. by Matthews and Caldeira (2007) and Bala et al. (2008). It can be explained from the latitude dependence of the forcing as discussed above. Also the seasonal dependence of the

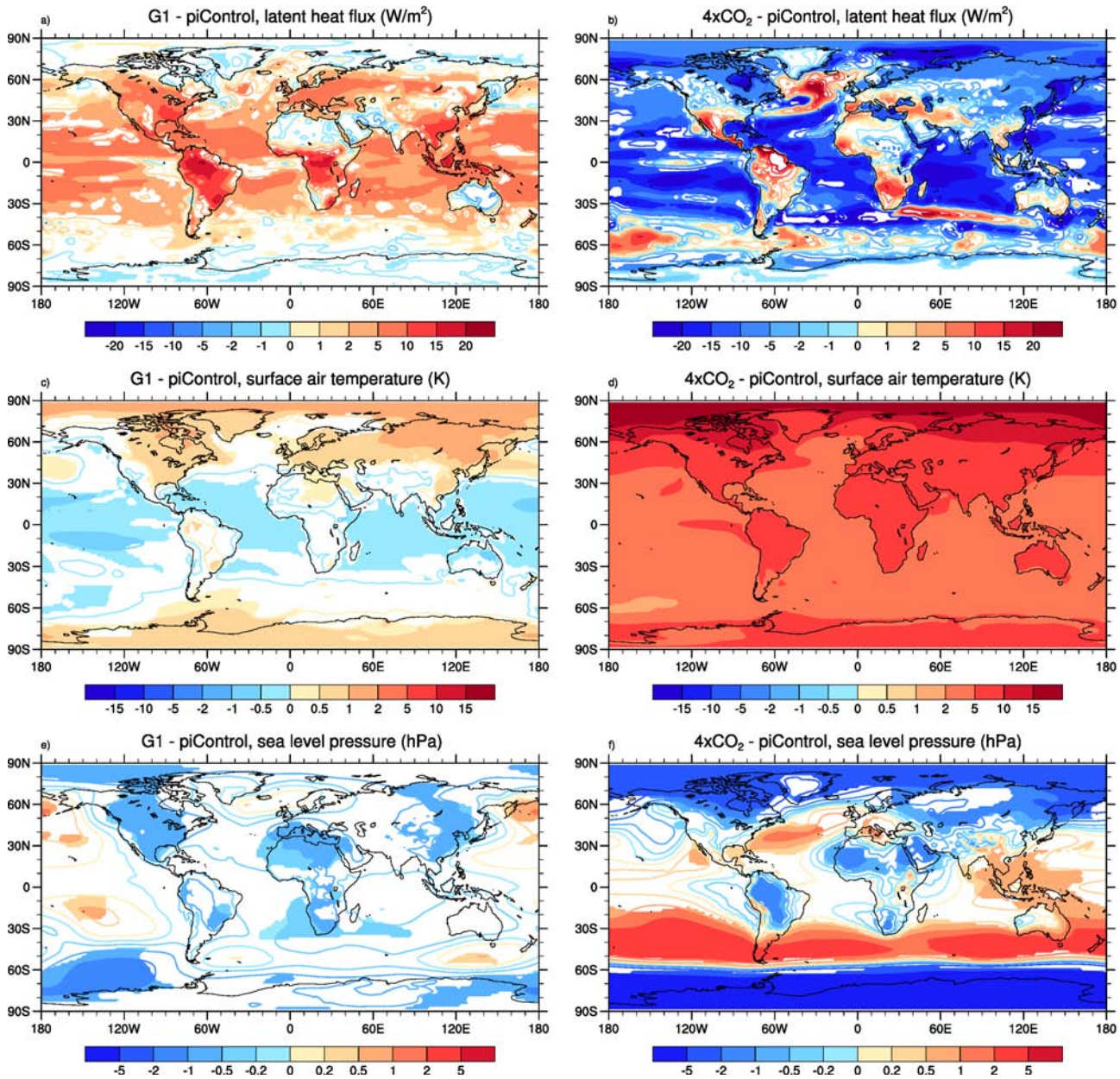

Fig. 3. Differences between the simulations G1 and piControl (left), and abrupt4xCO2 and piControl (right), averaged over the four ESMs. Top panels: surface latent heat flux ($W\,m^{-2}$; defined as positive downward), middle panels: near surface air temperature (K), and bottom panels: sea level pressure (hPa). In regions with filled color shading all models agree in the sign of the response. The value represented by the contours is given by the upper edge of the respective range in the color bar, i.e. the zero line is colored light blue.

temperature response (Fig. 6) can be explained directly with the seasonal dependence of the forcing. In general, high latitudes warm more in winter when the effect of the reduction of the solar constant is weak. The regional pattern of the annually-averaged SAT response (Fig. 3c) largely reflects the meridional gradient. Additionally, clear land-sea differences can be identified. The response over most continental land masses is more positive than over adjacent oceans. This is likely caused by the larger response of the latent heat flux over land, which is weakened more and hence results in less cooling than over the oceans.

4.3 Sea level pressure

Differences in sea level pressure between simulations G1 and piControl are in general small. The multi-model mean difference as shown in Fig. 3e has local maxima that are about an order of magnitude smaller than differences between the climate under CO_2 quadrupling and piControl

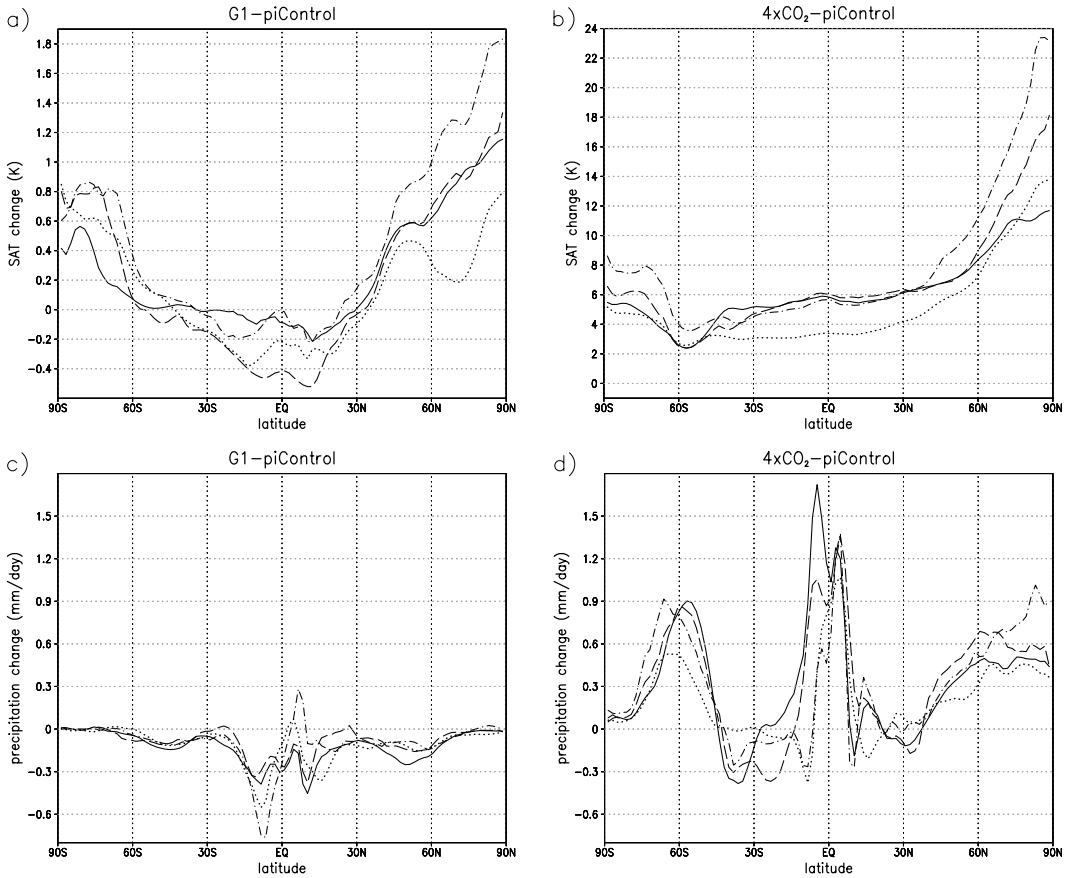

Fig. 4. Differences in zonally-averaged quantities between the simulations G1 and piControl (left panels), and abrupt4xco2 and piControl (right panels) from the four ESMs. Top panels: near surface air temperature (K), bottom panels: precipitation (mm day^{-1}). Solid: IPSL-CM5A, dashed: MPI-ESM, dotted: NorESM, dot-dashed: HadGEM2-ES. Note the different scaling of the temperature axes in the top panels.

(Fig. 3f). However, in some regions the differences are robust in the sense that all four ESMs show the same sign. This is in particular the case in the southern ocean west of the Antarctic peninsula with negative anomalies in G1 of the order of 1 hPa. In general, at high southern latitudes the signal indicates a weak poleward shift of the storm tracks as expected (although much stronger) under global warming (Meehl et al., 2007). This change in the circulation system can be expected to contribute to the surface temperature response pattern, e.g. to the stronger than average warming of the Antarctic peninsula. In the northern hemisphere, robust response patterns are the slight weakening of the low pressure systems over the Aleutians and in the North Atlantic. However, in the latter region only a tiny patch southwest of Iceland is robustly positive, and the single models predict fairly different locations of the centers of their high pressure anomalies (not shown). This means that fairly different responses of the North-Atlantic Oscillation (NAO) and north-western European climate are simulated in the different ESMs.

4.4 Precipitation

Under scenario G1 global mean precipitation is reduced in all four ESMs by values between 0.11 and 0.16 mm day^{-1}, or 3.6 to 6.1 % (see Table 3). Global reductions of precipitation have been predicted also by Govindasamy et al. (2003, 3.2 %) and Lunt et al. (2008, 5 %) under balanced quadrupling of CO_2. Bala et al. (2008) simulated a reduction of 1.7 % for balanced CO_2 doubling and discussed the reasons for the weakening of the global hydrological cycle. They argue (see discussion of latent heat flux, above) that while CO_2 forcing acts on the entire troposphere the solar forcing acts strongly on the surface. To balance the surface energy budget, a reduction of the latent heat flux occurs that requires under the assumption of a steady state which is well justified for long-term averages also a reduction of precipitation in the global mean.

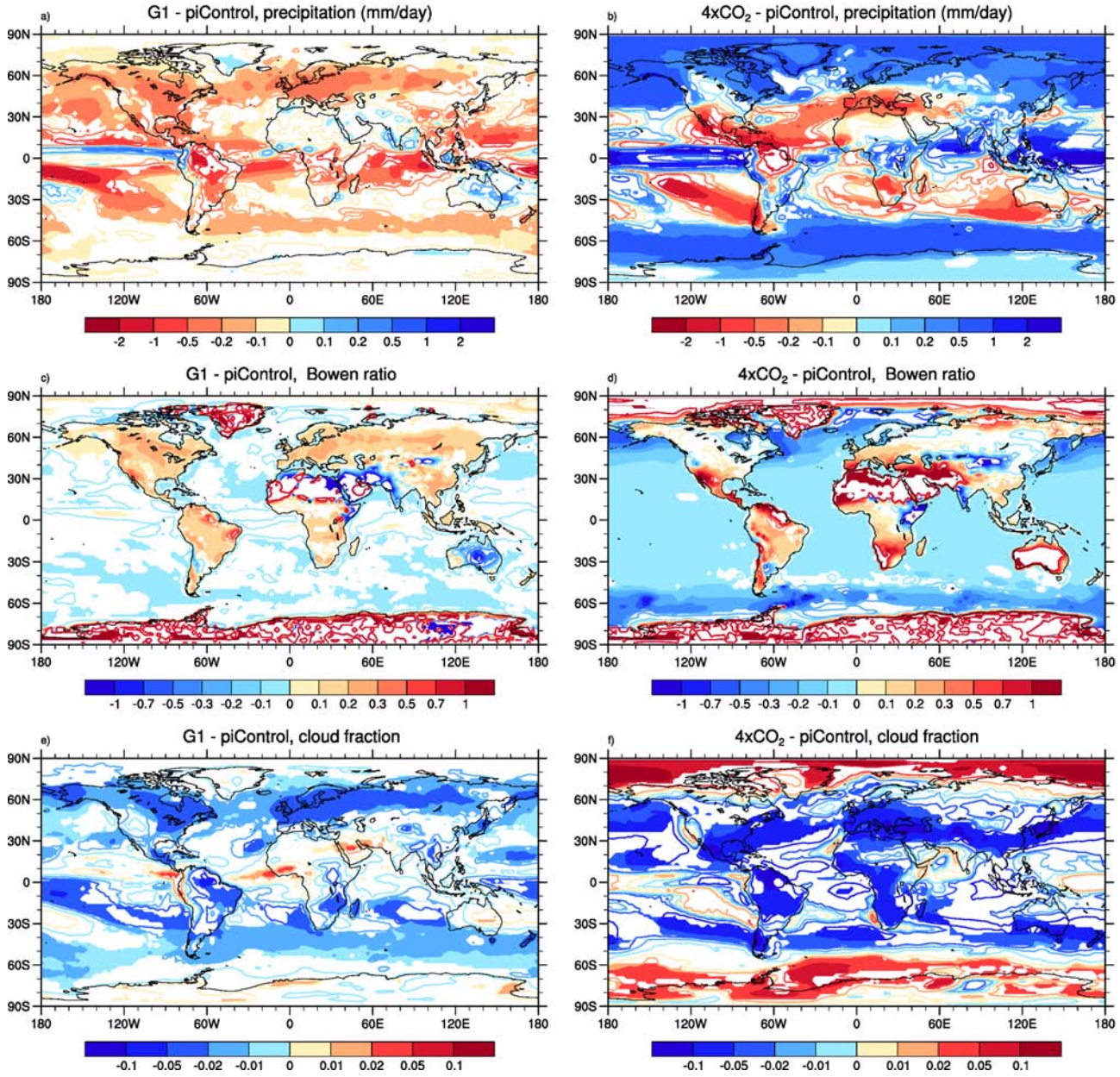

Fig. 5. Differences between the simulations G1 and piControl (left), and abrupt4xco2 and piControl (right), averaged over the four ESMs. Top panels: precipitation (mm day^{-1}), middle panels: Bowen ratio (ratio of surface sensible and latent heat fluxes), and bottom panels: total cloud fraction. In regions with filled color shading all models agree in the sign of the response. The value represented by the contours is given by the upper edge of the respective range in the color bar, i.e. the zero line is colored light blue (light yellow in the case of precipitation).

The zonally-averaged response of precipitation has similar patterns for all four ESMs (Fig. 4c). In general, the models show local response maxima in the mid-latitudes of both hemispheres close to about 50° with reductions of about 0.1 to 0.15 mm day^{-1}, i.e. about 4 % in the southern hemisphere and between 0.1 and 0.25 mm day^{-1}, or 6 to 12 %, in the northern hemisphere. We conjecture that the reduced mid-latitude precipitation is linked to (a) less evaporation in the tropics and (b) the reduced meridional temperature gradient. Branscome and Gutowski (1992) have suggested from sensitivity simulations that a reduced meridional temperature gradient (from doubling of CO_2 in their case) would lead to weaker eddy transport of heat and weaker subtropical transport of water vapor. The reduction of latent heat flux in particular over continents contributes to the pattern of the precipitation change. The strongest absolute changes in precipitation occur in the tropics where precipitation rates are highest. Depending on the model also the highest relative

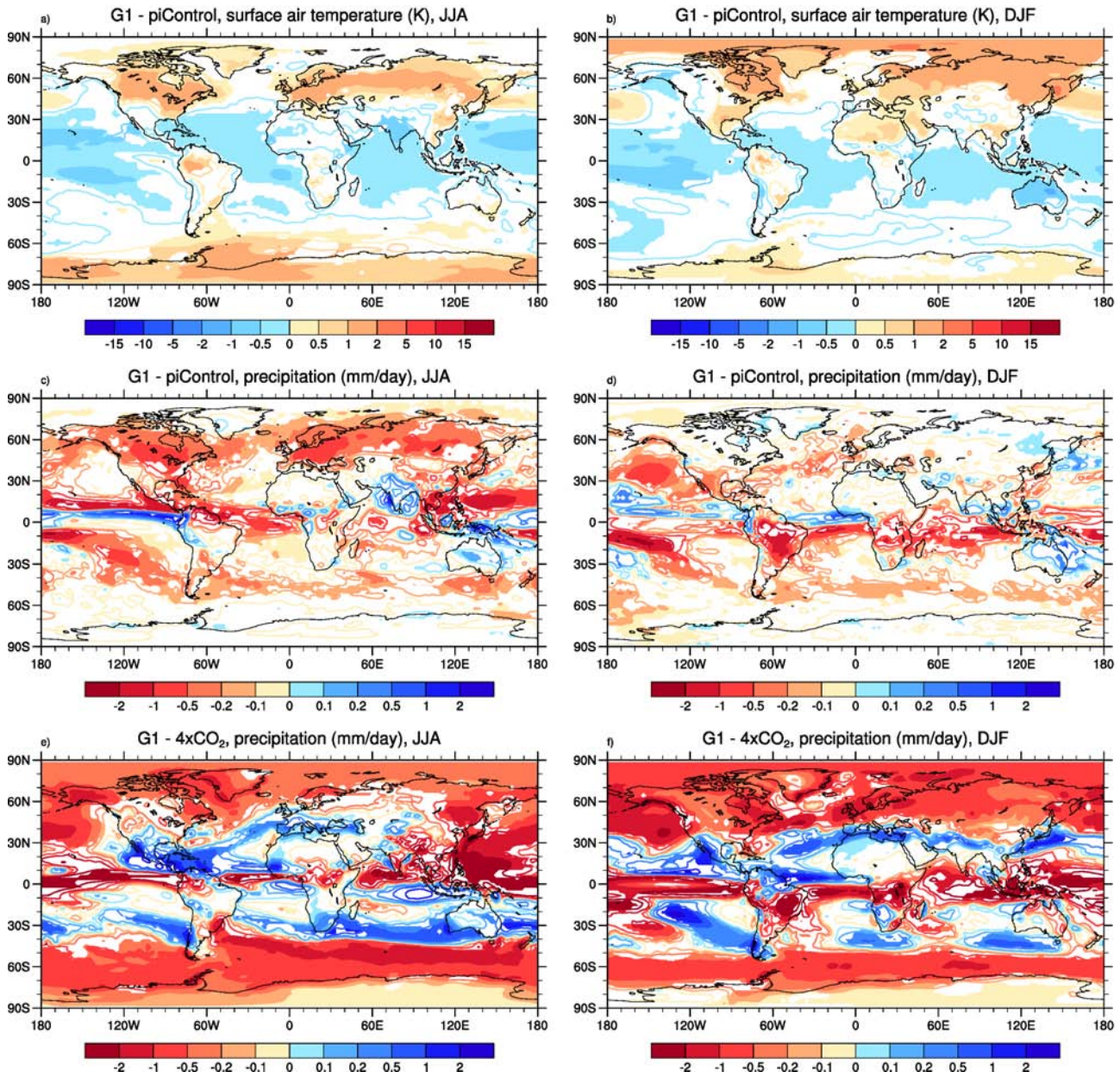

Fig. 6. Differences in near surface air temperature (K, top panels) and precipitation (mm day^{-1}, middle panels) between the simulations G1 and piControl, and in precipitations between the simulations G1 and abrupt4xCO2 (mm day^{-1}, bottom panels). All quantities are averaged over the four ESMs and the seasons June-July-August (JJA, left column) and December-January-February (DJF, right column), respectively. In regions with filled color shading all models agree in the sign of the response. The value represented by the contours is given by the upper edge of the respective range in the color bar, i.e. the zero line is colored light blue in the case of temperature and light yellow in the case of precipitation.

changes of up to 20 % (both negative and positive) are simulated in this region. All models show qualitatively similar patterns with strong reductions in the southern branch of the inter-tropical convergence zone (ITCZ), a local response maximum directly north of the equator, and, except for HadGEM2-ES, also a clear minimum in the ITCZ branch north of the equator. While in HadGEM2-ES the zonally-averaged position of the main branch of the ITCZ remains almost unchanged, it shifts slightly equatorward in the other three models. The tropical signals have to be interpreted with caution, as all four ESMs, to various degrees, suffer from the double-ITCZ problem common for this type of models (Randall et al., 2007).

Table 4. Comparison of differences between the $4x \times CO_2$ and preindustrial climates (abrupt4xCO2 – piControl) in globally-averaged parameters. Note that in the case of $4 \times CO_2$, averages are calculated over years 101 to 150, during which the simulated climate has not yet reached an equilibrium.

	IPSL-CM5A	MPI-ESM	NorESM	HadGEM2-ES
TOA net flux ($W\,m^{-2}$)	1.9	1.8	1.9	1.9
SAT (K)	5.7	5.9	4.1	6.3
Precipitation ($mm\,day^{-1}$)	0.32 (11.9 %)	0.29 (9.8 %)	0.17 (5.9 %)	0.23 (7.4 %)
Cloud fraction	−0.056 (−9.6 %)	−0.028 (−4.3 %)	0.009 (1.7 %)	−0.017 (−3.3 %)
Planetary albedo	−0.029 (−9.4 %)	−0.014 (−4.4 %)	−0.012 (−3.7 %)	−0.020 (−6.5 %)

Table 5. Comparison of multi-model mean responses to the forcings in G1 and abrupt4xCO2 simulations, respectively, with respect to piControl. Responses are calculated for the individual models both in terms of spatially averaged differences and in terms of root mean square differences, and then averaged over the four ESMs. RMS differences are calculated after interpolation of the results from the individual models to a 192×96 grid. Besides global mean values, also averages over land surface only are provided.

	SAT (K)		Precipitation ($mm\,day^{-1}$)	
	G1	4xCO2	G1	4xCO2
global average	0.1	5.5	−0.14	0.25
(percentage)			(−4.7 %)	(8.8 %)
land average	0.4	7.5	−0.12	0.16
(percentage)			(−6.3 %)	(8.3 %)
rms (global)	0.5	6.1	0.35	0.91
(percentage)			(12.2 %)	(31.6 %)
rms (land)	0.7	7.7	0.31	0.68
(percentage)			(16.4 %)	(36.4 %)

The local maxima of zonal average precipitation reduction in the middle to high latitudes dominate also the regional pattern of the precipitation response as presented in Fig. 5a. In both hemispheres zonal bands can be identified where all models predict a reduction. While in the southern hemisphere this concerns the oceans, large land masses are affected in the northern hemisphere. Precipitation is reduced in the multi-model average by about 0.2 to 0.4 $mm\,day^{-1}$ (10 to 20 %) in a large part of eastern North America and a large zonal band over northern Eurasia. In these regions, the strongest reduction (of more than 0.5 $mm\,day^{-1}$ in large areas) is occuring during the summer months (see Fig. 6). In the tropics and sub-tropics the patterns are more complicated and in particular over the Indian subcontinent and over South-East Asia the models disagree on the sign of the response. This is true also for large parts of Africa and Australia. Over central South America, all models show a decrease of precipitation that reaches more than 20 % in parts of the Amazon region. While the multi-model average shows reductions of about 0.5 $mm\,day^{-1}$ over a large area, single models differ considerably in the magnitude. The strongest reductions of precipitation over central South America, reaching more than 2 $mm\,day^{-1}$ locally, are predicted by the IPSL-CM5A and HadGEM2-ES. In the northernmost part of the Andes, precipitation increases most in the NorESM (up to 3 $mm\,day^{-1}$). Over the tropical oceans reductions of precipitation dominate except for a small band slightly north of the equator over the Pacific which indicates an equatorward shift of the ITCZ in three of four models as mentioned above.

The simulated reduction of precipitation over large land areas is not necessarily an indicator for a decrease of water availability or an increase of droughts as the latent heat fluxes are also reduced. The difference between precipitation and evaporation ($P - E$) is often considered a better parameter. Indeed, in the multi-model average, in agreement with findings from Govindasamy et al. (2003), $P - E$ (not shown) decreases in large parts of the land areas that show a decrease in precipitation; however, the responses are in large areas not robust among all four ESMs. Another indicator for dry- and wetness of land masses is the Bowen ratio (ratio of sensible to latent heat flux). Dry continents generally have Bowen ratios above one and wet continents below one. As shown in Fig. 5c the Bowen ratio increases robustly over those regions that also show a decrease of precipitation. This is an indication for increasing dryness of large continental regions.

It should be noted that the global mean reduction of precipitation is specific to the scenario studied here and not necessarily a generic feature of any SRM. One could attempt to design a scenario aiming at the compensation of the global-mean or land-mean precipitation increase caused by the CO_2 increase, but in such a case the temperature increase would be less well compensated.

4.5 Cloud cover

The total global cloud fraction is reduced under scenario G1 in all four models by values between 0.006 and 0.010 (i.e. 1.1 to 1.7 %, see Table 3). While the response of high clouds differs among the ESMs, the cloud fraction of low clouds is reduced in all four models over almost all latitudes. This reduction contributes to the change of the planetary albedo that is also reduced in all four models by between 0.006 and 0.009 (1.8 to 2.6 %). As mentioned earlier, this response of the cloud fraction also contributes to the solar forcing being less effective than the CO_2 forcing. To identify the reason for the response of clouds to forcing in the G1

scenario is beyond the scope of this work but should be the aim of future studies.

Similar to the change in precipitation, the reduction in cloud fraction is simulated in all models in middle to high latitude zonal bands in both hemispheres including the storm tracks (see Fig. 5e). A particularly strong multi-model mean reduction of the cloud fraction with values up to 0.03 is predicted for western and central Europe. In large parts of the tropics and sub-tropics, the models tend to disagree in the sign of the change. Regions of strongly decreasing cloud fraction in all models are the north-east of central South America and the western tropical Pacific.

5 Climate response to unmitigated quadrupling of CO_2 in comparison with the response to CE

The abrupt4xCO2 experiment is an official CMIP5 experiment and we expect that it will be analyzed in detail elsewhere. The intention of this section is to provide a short overview of selected results of this experiment in order to allow a comparison of the climate response under CE with unmitigated climate change. Table 4 contains responses to CO_2 quadrupling of selected global mean parameters and can be compared directly to Table 3. Table 5 presents multi-model average responses in SAT and precipitation from both scenarios (G1 and abrupt4xCO2) in terms of both mean and root mean square (rms) differences. Additionally, not only global means but also averages over all land surfaces are presented. It should be repeated that the abrupt4xCO2 simulation is still not in equilibrium during years 101 to 150, which are used here. This is evident from the difference in TOA net flux imbalances between abrupt4xCO2 and piControl listed in the first line of Table 4.

The global temperature response to CO_2 quadrupling lies between 5.7 and 6.3 K for three of the four ESMs but is significantly lower in the NorESM (4.1 K). The reduction of the solar constant in experiment G1 compensates this temperature increase almost completely, as can be expected from the design of the experiment. Figure 4b shows the latitudinal dependence of the zonally-averaged temperature response in experiment abrupt4xCO2. All four ESMs show stronger responses at NH high latitudes than in the other regions. While the three models with comparable climate sensitivity show very similar responses in the tropics and sub-tropics, the NorESM warms about 2 to 3 K less at these latitudes. Different polar amplifications across the models lead to temperature increases at the North Pole between about 11 K (IPSL-CM5A) and 23 K (HadGEM2). The latitudinal structure of the temperature response under CE is similar to the response in abrupt4xCO2 but much smaller in magnitude with polar warmings of the order of 1 K, and of course the opposite sign (cooling) in the tropics. While the low-latitude response of the NorESM is significantly different under CO_2 quadrupling it is well within the range of the other three models in G1. Table 5 confirms (cf. Sect. 4.2 and Fig. 3) that in both scenarios the temperatures over land areas increase stronger than in the global mean, but in the case of G1 the average temperature response over land is small (0.4 K). When expressed as rms differences, multi-model mean changes of SAT under G1 are about an order of magnitude smaller than under abrupt4xCO2. This is true for both land and global mean responses.

In contrast to temperature, global mean precipitation changes strongly both with and without balancing of the CO_2 forcing. While the change is strongly positive in abrupt4xCO2 (increases between 5.9 and 11.9 % compared to piControl; 8.8 % in the multi-model mean), it is strongly negative in G1 with reductions that range between 3.6 and 6.1 % (4.7 % in the multi-model mean). The precipitation increase due to quadrupling of CO_2 is, hence, strongly overcompensated in G1. Regionally, precipitation responses in G1 can be of the same magnitude as in abrupt4xCO2 even in the multi-model mean (Fig. 5). For instance, in the eastern part of North America and in parts of northern Eurasia an increase caused by CO_2 is turned into a decrease of similar magnitude by CE. By contrast, for the Mediterranean the models show a robust decrease of precipitation as a climate change signal and no robust signal after CE. The response of the Bowen ratio to quadrupling of CO_2 (Fig. 5d) indicates increasing dryness everywhere around the Mediterranean while under G1 the Bowen ratio responds less uniformly. In the northern part of the Amazon region, both experiments show a strong decrease of precipitation which is of larger magnitude in the multi-model ensemble of abrupt4xCO2 albeit also less robust than in G1. Table 5 shows that the magnitude of precipitation responses in the two scenarios is more similar for land masses only (−6.3 % in G1, vs. 8.3 % in abrupt4xCO2) than for the full global average. In terms of rms differences the CE in G1 reduces the precipitation anomalies caused in abrupt4xCO2 by a factor of 2.6 in the global mean and 2.2 over land surfaces.

As mentioned earlier, responses in sea level pressure to quadrupling of CO_2 are strongly reduced through the reduction of solar irradiance in G1 (cf. Fig. 3e and f). Regional response maxima are smaller by almost an order of magnitude in G1 than in abrupt4xCO2. In three of four models, a reduction of the responses, although less strong, is also predicted for globally-averaged cloud fraction (Table 4). The signal, which ranges from −9.6 to +1.7 % for quadrupling of CO_2, is changed to a range from −1.7 to −1.1 % through the balancing (cf. Tables 3 and 4). Interestingly, the responses to CO_2 forcing alone differ significantly more across the models than the responses in G1, hinting at model specific feedbacks which become relevant at the higher temperature changes of the abrupt4xCO2 experiment. The NorESM is the only model that predicts a positive response of cloud fraction in abrupt4xCO2. This may explain, at least partly, the smaller climate sensitivity of the NorESM. The sign of the cloud fraction response in the NorESM is reversed in

G1, i.e. negative as for the other three ESMs. The planetary albedo is reduced in all models as a response to the CO_2 forcing. This is true also for the NorESM despite the simulated increase in total cloud fraction. Reduced snow and ice cover in abrupt4xCO2 contribute to this reduction of the planetary albedo.

6 Responses of monsoon systems to CE

A frequently discussed question is the potential response of monsoon circulations and precipitation to CE. Robock et al. (2008) have predicted a weakening of Asian and African summer monsoon circulations as a response to CE via sulfur emissions at both tropical and high northern latitudes. Figure 6c shows the differences between geoengineered and preindustrial JJA precipitation as an average from the four ESMs in this study. In most monsoon regions the four models disagree on the sign of the response. Only in some parts of south-east Asia is a robust decrease of precipitation simulated. In the case of India, the multi-model average indicates an increase of JJA precipitation along with an increase in cloud fraction (not shown) and, as a consequence, a robust decrease in temperature (Fig. 6a). The monsoon circulation depends on the land-sea temperature gradient, and an increase may be expected with generally increasing land-sea differences under G1. However, while the Indian ocean robustly cools, a robust warming is simulated only for the northern part of the Asian continent. The temperature decrease over India in JJA may be interpreted as a response to the changing monsoon, but also in pre-monsoon months (not shown) no robust warming is simulated over the southern part of the Asian continent. In contrast to our G1 response, Robock et al. (2008) have simulated a general decrease of temperatures over Asian land masses and a decrease of Indian monsoon precipitation as observed also for high-latitude volcanic eruptions (Oman et al., 2005, 2006). However, Robock et al. (2008) compare a CE scenario with respect to an unmitigated future scenario. A more appropriate comparison is hence the precipitation response in G1 with respect to the unmitigated abrupt4xCO2 scenario (Fig. 6e). In this case as well, the four models generally do not agree on the sign of the precipitation response. Over central and southern India the average response is, however, a decrease in precipitation which points in the same direction as the simulations by Robock et al. (2008).

7 Summary and conclusions

In this study we have compared the response of four state-of-the-art Earth system models, which are also employed for the CMIP5 simulations, to climate engineering under scenario G1 of the Geoengineering Model Intercomparison Project (GeoMIP). G1 is not intended to be a realistic scenario for a potential future application of CE. However, the instantaneous quadrupling of CO_2 and its balancing by a strong reduction of total solar irradiance provide strong and easy to simulate forcings. This allows us to clearly identify and compare basic responses of the climate system without having to consider potential differences related to the degree of sophistication by which, for example, aerosol-based CE methods may be implemented in different models.

The following selection of model responses has been simulated robustly among all four models in experiment G1.

- Solar forcing is less effective than the forcing caused by the increase of CO_2. This is related to the decrease of cloud cover in the geoengineered climate. Consequently, depending on the model, between 18 and 38 % "more" CE than expected had to be implemented.
- The latitudinal dependence of solar and CO_2 forcing leads to a latitudinal gradient in TOA net radiation balance anomaly.
- The globally-averaged temperature is kept almost constant but the meridional temperature gradient is reduced. Polar regions are still warmer than the pre-industrial control simulation by about 1 K, while the tropics are slightly cooler. On average, land masses show a more positive temperature response than adjacent oceans. The residual polar warming is much weaker than under unbalanced quadrupling of the CO_2 concentration.
- In the surface energy budget, the decrease of incoming solar radiation is largely balanced by a decrease in the latent heat flux. This decrease is particularly strong over vegetation-covered land masses.
- As a consequence of the reduced water vapor flux, globally-averaged precipitation decreases on average by 4.7 %. In particular, a strong decrease is simulated for large areas of North America, northern Eurasia and central South America.
- Globally averaged precipitation changes simulated for the quadrupled CO_2 scenario are about a factor of two larger in magnitude, but of opposite sign than the precipitation change for the G1 scenario. Over land masses the precipitation changes under G1 and abrupt4xCO2 are less different in magnitude than over sea. Regionally, changes in precipitation may even increase through CE.

Similar responses have been predicted in earlier single-model studies of a balancing of CO_2 increase by a reduction of the solar constant (see references in the introduction). The comparison of four climate models of the current generation simulating exactly the same scenario allows us to better quantify and assess the uncertainties of the response. Besides the robust responses mentioned above, the models also show strong disagreement in other parameters and areas. Precipitation responses over tropical and subtropical land areas may

be strongly positive in one and strongly negative in another model. This highlights the need to improve the simulation of precipitation in climate models not only for the purpose of estimating potential consequences of CE, but also to improve climate predictions in general.

This study has only addressed a small number of climate parameters. We have not discussed potentially important responses of the oceans (including sea ice), the carbon cycle, vegetation, the dynamics and chemistry of the middle atmosphere, and the diurnal cycles of temperature and precipitation. Other modeling centers have expressed their interest in simulating the GeoMIP experiment G1, so that future studies of these parameters may be based on an even more representative model ensemble. This study, however, allows us to conclude that climate engineering via solar radiation management (in this case by reducing the solar constant, equivalent to deploying hypothetical space mirrors) aiming at the restoration of the globally-averaged temperature of a past climate state (preindustrial in our case) would certainly lead to significant changes in other climate parameters. In particular, strongly changed global mean and regional precipitation can be expected. Other scenarios, e.g. a restoration of global mean precipitation could be envisaged, but would then restore the temperature less well.

SRM techniques other than the reduction of the solar constant have been much discussed in the recent past, in particular the artificial injection of aerosols into the stratosphere. It is unclear to what extent this technique under a more realistic scenario would lead to responses comparable to those presented here. However, other GeoMIP scenarios (Kravitz et al., 2011b) specific to this technique will be calculated by several modeling groups and will thereby allow a better assessment of potential consequences.

The climate response to climate engineering as opposed to a situation with unmitigated greenhouse gas emissions may be detrimental for the populations and ecosystems in some regions and beneficial in other regions. Impact studies would be needed to estimate the effects, e.g. of precipitation responses such as the reduction over large northern land masses simulated under the G1 scenario. It may be tempting to "optimize" CE in order to minimize changes in temperature and precipitation (Ban-Weiss and Caldeira, 2010). Note, for instance, that the difference in latitudinal dependence of solar and CO_2 forcing resulted in a latitudinal gradient in the net TOA fluxes in our simulations, which might be avoidable with an adapted solar forcing pattern. However, the strong change in precipitation in the G1 experiment would probably not disappear with an optimized solar forcing pattern. Also, from the different responses among the models with respect to precipitation in low-latitude regions, it is obvious that the current generation of climate models will not allow an exact prediction of the outcome of CE measures, and as stated by Robock et al. (2010), due to the large internal variability of weather and climate, CE "cannot be tested without full scale implementation". Model simulations by MacMynowski et al. (2010) indicate that tests with forcing modulated in periods of a few years may help to reduce the risk of extreme responses, but also that responses to long-term implementation may differ from those estimated from periodic tests. Another risk of solar radiation management is the expected rapid climate change after a potential abrupt termination. This will be studied in other GeoMIP experiments.

The climate response is only one aspect that has to be considered if the implementation of CE techniques is discussed. Other potential side effects specific to some methods, as well as political, ethical, legal and economical implications have to be taken into account. But the potentially strong climate responses discussed here suggest that climate engineering cannot be seen as a substitute for a policy pathway of mitigating climate change through the reduction of greenhouse gas emissions.

Acknowledgements. The research leading to these results has received funding from the European Union's Seventh Framework Programme (FP7/2007-2013) under grant agreement no. 226567-IMPLICC. This work was performed using HPC resources from GENCI-[CCRT/TGCC/CINES/IDRIS] (Grant 2012-t2012012201). A. J. was supported by the Joint DECC/Defra Met Office Hadley Centre Climate Programme (GA01101). H. S., U. N. and C. T. would like to thank the MPI-ESM development team and the DKRZ where the simulations with the MPI-ESM have been performed and archived. D. B. K. thanks the IPSL-CM5A development team for support in realizing the simulations. A. K. and J. E. K. thank the Norwegian Research Council's Programme for Supercomputing for support through a grant of computing time.

Edited by: G. Bala

References

Alterskjær, K., Kristjánsson, J. E., and Seland, Ø.: Sensitivity to deliberate sea salt seeding of marine clouds – observations and model simulations, Atmos. Chem. Phys., 12, 2795–2807, doi:10.5194/acp-12-2795-2012, 2012.

Assmann, K. M., Bentsen, M., Segschneider, J., and Heinze, C.: An isopycnic ocean carbon cycle model, Geosci. Model Dev., 3, 143–167, doi:10.5194/gmd-3-143-2010, 2010.

Bala, G., Duffy, P. B., and E., T. K.: Impact of geoengineering schemes on the global hydrological cycle, P. Natl. Acad. Sci. USA, 105, 7664–7669, doi:10.1073/pnas.0711648105, 2008.

Ban-Weiss, G. A. and Caldeira, K.: Geoengineering as an optimization problem, Environ. Res. Lett., 5, 034009, doi:10.1088/1748-9326/5/3/034009, 2010.

Branscome, L. E. and Gutowski, W. J.: The impact of doubled CO_2 on the energetics and hydrologic processes of mid-latitude transient eddies, Clim. Dynam., 8, 29–37, doi:10.1007/BF00209341, 1992.

Budyko, M. I.: Climatic changes, American Geophysical Society, Washington, D.C., doi:10.1029/SP010, 1977.

Collins, W. J., Bellouin, N., Doutriaux-Boucher, M., Gedney, N., Halloran, P., Hinton, T., Hughes, J., Jones, C. D., Joshi, M., Liddicoat, S., Martin, G., O'Connor, F., Rae, J., Senior, C., Sitch,

S., Totterdell, I., Wiltshire, A., and Woodward, S.: Development and evaluation of an Earth-System model – HadGEM2, Geosci. Model Dev., 4, 1051–1075, doi:10.5194/gmd-4-1051-2011, 2011.

Crutzen, P. J.: Albedo enhancement by stratospheric sulfur injections: A contribution toresolve a policy dilemma?, Climatic Change, 77, 211–219, 2006.

Dufresne, J.-L., Foujols, M.-A., Denvil, S., Caubel, A., Marti, O., Aumont, O., Balkanski, Y., Bekki, S., Bellenger, H., Benshila, R., Bony, S., Bopp, L., Braconnot, P., Brockmann, P., Cadule, P., Cheruy, F., Codron, F., Cozic, A., Cugnet, D., de Noblet, N., Duvel, J.-P., Ethé, C., Fairhead, L., Fichefet, T., Flavoni, S., Friedlingstein, P., Grandpeix, J.-Y., Guez, L., Guilyardi, E., Hauglustaine, D., Hourdin, F., Idelkadi, A., Ghattas, J., Joussaume, S., Kageyama, M., Krinner, G., Labetoulle, S., Lahellec, A., Lefebvre, M.-P., Lefevre, F., Levy, C., Li, Z. X., Lloyd, J., Lott, F., Madec, G., Mancip, M., Marchand, M., Masson, S., Meurdesoif, Y., Mignot, J., Musat, I., Parouty, S., Polcher, J., Rio, C., Schulz, M., Swingedouw, D., Szopa, S., Talandier, C., Terray, P., and Viovy, N.: Climate change projections using the IPSL-CM5 Earth System Model: from CMIP3 to CMIP5, Climate Dynam., submitted, 2012.

Essery, R. L. H., Best, M. J., Betts, R. A., Cox, P. M., and Taylor, C. M.: Explicit representation of subgrid heterogeneity in a GCM land surface scheme, J. Hydrometeorol., 4, 530–543, 2003.

GAO: Technology asessment: Climate Engineering: Technical status, future directions and potential responses, US Government Accountability Office, Washington, USA, 2011.

Giorgetta, M. A., Jungclaus, J., Reick, C., Stevens, B., Marotzke, J., Claussen, M., Roeckner, E., Mauritsen, T., Crueger, T., Schmidt, H., Manzini, E., Esch, M., Rast, S., Kinne, S., Zhang, K., Kornblueh, L., Haak, H., Segschneider, J., Six, K., Raddatz, T., Gayler, V., Schnur, R., Legutke, S., Widmann, H., and Glushak, K.: Climate variability and climate change in MPI-ESM CMIP5 simulations, in preparation, 2012.

Govindasamy, B. and Caldeira, K.: Geoengineering Earth's radiation balance to mitigate climate change, Geophys. Res. Lett., 27, 2141–2144, 2000.

Govindasamy, B., Caldeira, K., and Duffy, P. B.: Geoengineering Earth's radiation balance to mitigate climate change from a quadrupling of CO_2, Global Planet. Change, 37, 157–168, 2003.

Gregory, J. and Webb, M.: Tropospheric adjustment induces a cloud component in CO_2 forcing, J. Climate, 21, 58–71, doi:10.1175/2007JCLI1834.1, 2008.

Gregory, J. M., Ingram, W. J., Palmer, M. A., Jones, G. S., Stott, P. A., Thorpe, R. B., Lowe, J. A., Johns, T. C., and Williams, K. D.: A new method for diagnosing radiative forcing and climate sensitivity, Geophys. Res. Lett., 310, L03205, doi:10.1029/2003GL018747, 2004.

Hansen, J., Sato, M., and Ruedy, R.: Radiative forcing and climate response, J. Geophys. Res., 102, 6831–6864, doi:10.1029/96JD03436, 1997.

Hansen, J., Sato, M., Ruedy, R., Nazarenko, L., Lacis, A., Schmidt, G. A., Russell, G., Aleinov, I., Bauer, M., Bauer, S., Bell, N., Cairns, B., Canuto, V., Chandler, M., Cheng, Y., Del Genio, A., Faluvegi, G., Fleming, E., Friend, A., Hall, T., Jackman, C., Kelley, M., Kiang, N., Koch, D., Lean, J., Lerner, J., Lo, K., Menon, S., Miller, R., Minnis, P., Novakov, T., Oinas, V., Perlwitz, J., Perlwitz, J., Rind, D., Romanou, A., Shindell, D., Stone, P., Sun, S., Tausnev, N., Thresher, D., Wielicki, B., Wong, T., Yao, M., and Zhang, S.: Efficacy of climate forcings, J. Geophys. Res., 110, D18104, doi:10.1029/2005JD005776, 2005.

Hourdin, F., Foujols, M.-A., Codron, F., Guemas, V., Dufresne, J.-L., Bony, S., Denvil, S., Guez, L., Lott, F., Ghattas, J., Braconnot, P., Marti, O., Meurdesoif, Y., and Bopp, L.: Impact of the LMDZ atmospheric grid configuration on the climate and sensitivity of the IPSL-CM5A coupled model, Clim. Dynam., in press, 2012.

Irvine, P. J., Ridgwell, A., and Lunt, D. J.: Assessing the regional disparities in geoengineering impacts, Geophys. Res. Lett., 37, L18702, doi:10.1029/2010GL044447, 2010.

Jones, A., Haywood, J., Boucher, O., Kravitz, B., and Robock, A.: Geoengineering by stratospheric SO_2 injection: results from the Met Office HadGEM2 climate model and comparison with the Goddard Institute for Space Studies ModelE, Atmos. Chem. Phys., 10, 5999–6006, doi:10.5194/acp-10-5999-2010, 2010.

Joshi, M. and Gregory, J.: Dependence of the land-sea contrast in surface climate response on the nature of the forcing, Geophys. Res. Lett., 352, L24802, doi:10.1029/2008GL036234, 2008.

Kravitz, B., Robock, A., Boucher, O., Schmidt, H., and Taylor, K.: Specifications for GeoMIP experiments G1 through G4 (frozen version: 1.0), http://climate.envsci.rutgers.edu/GeoMIP/docs/specificationsG1_G4_v1.0.pdf (last access: 31 May 2012), 2011a.

Kravitz, B., Robock, A., Boucher, O., Schmidt, H., Taylor, K., Stenchikov, G., and Schulz, M.: The Geoengineering Model Intercomparison Project (GeoMIP), Atmos. Sci. Lett., 12, 162–167, doi:10.1002/asl.316, 2011b.

Krinner, G., Viovy, N., de Noblet-Ducoudré, N., Ogée, J., Polcher, J., Friedlingstein, P., Ciais, P., Sitch, S., and Prentice, I. C.: A dynamic global vegetation model for studies of the coupled atmosphere-biosphere system, Global Biogeochem. Cy., 19, GB1015, doi:10.1029/2003GB002199, 2005.

Latham, J.: Control of global warming?, Nature, 347, 339–340, 1990.

Lenton, T. M. and Vaughan, N. E.: The radiative forcing potential of different climate geoengineering options, Atmos. Chem. Phys., 9, 5539–5561, doi:10.5194/acp-9-5539-2009, 2009.

Lunt, D. J., Ridgwell, A., Valdes, P. J., and Seale, A.: "Sunshade World": A fully coupled GCM evaluation of the climatic impacts of geoengineering, Geophys. Res. Lett., 351, L12710, doi:10.1029/2008GL033674, 2008.

MacMynowski, D. G., Keith, D. W., Caldeira, K., and Shin, H.-J.: Can we test geoengineering?, Energy Environ. Sci., 4, 5044–5052, doi:10.1039/C1EE01256H, 2011.

Madec, G.: NEMO ocean engine, Tech. Rep. 27, Institut Pierre Simon Laplace des Sciences de l'Environnement Global, Paris, France, 2008.

Marsland, S. J., Haak, H., Jungclaus, J. H., Latif, M., and Röske, F.: The Max-Planck-Institute global ocean/sea ice model with orthogonal curvilinear coordinates, Ocean Modell., 5, 91–127, 2003.

Matthews, H. D. and Caldeira, K.: Transient climate carbon simulations of planetary geoengineering, P. Natl. Acad. Sci. USA, 104, 9949–9954, doi:10.1073/pnas.0700419104, 2007.

Mautner, M.: A space-based solar screen against climate warming, J. Brit. Interpl. Soc., 44, 135–138, 1991.

Meehl, G. A., Stocker, T. F., Collins, W. D., Friedlingstein, P., Gaye, A. T., Gregory, J. M., Kitoh, A., Knutti, R., Murphy, J. M., Noda,

A., Raper, S. C. B., Watterson, I. G., Weaver, A. J., and Zhao, Z.-C.: Global Climate Projections, in: Climate Change 2007: The Physical Science Basis, in: Contribution of Working Group I to the Fourth Assessment Report of the Intergovernmental Panel on Climate Change, edited by: Solomon, S., Qin, D., Manning, M., Chen, Z., Marquis, M., Averyt, K. B., Tignor, M., and Miller, H. L., Cambridge Univ. Press, New York, 747–845, 2007.

Moss, R. H., Edmonds, J. A., Hibbard, K. A., Manning, M. R., Rose, S. K., van Vuuren, D. P., Carter, T. R., Emori, S., Kainuma, M., Kram, T., Meehl, G. A., Mitchell, J. F. B., Nakicenovic, N., Riahi, K., Smith, S. J., Stouffer, R. J., Thomson, A. M., Weyant, J. P., and Wilbanks, T. J.: The next generation of scenarios for climate change research and assessment, Nature, 463, 747–756, doi:10.1038/nature08823, 2010.

Oleson, K. W., Lawrence, D. M., Bonan, G. B., Flanner, M. G., Kluzek, E., Lawrence, P. J., Levis, S., Swenson, S. C., and Thornton, P. E.: Technical Description of version 4.0 of the Community Land Model (CLM), Tech. Rep. NCAR/TN-478+STR, National Center for Atmospheric Research, Boulder, CO, USA, 2010.

Oman, L., Robock, A., Stenchikov, G., Schmidt, G. A., and Ruedy, R.: Climatic response to high-latitude volcanic eruptions, J. Geophys. Res., 110, D13103, doi:10.1029/2004JD005487, 2005.

Oman, L., Robock, A., Stenchikov, G. L., and Thordarson, T.: High-latitude eruptions cast shadow over the African monsoon and the flow of the Nile, Geophys. Res. Lett., 33, L18711, doi:10.1029/2006GL027665, 2006.

Pongratz, J., Lobell, D. B., Cao, L., and Caldeira, K.: Crop yields in a geoengineered climate, Nat. Clim. Change, 2, 101–105, doi:10.1038/nclimate1373, 2012.

Raddatz, T. J., Reick, C. H., Knorr, W., Kattge, J., Roeckner, E., Schnur, R., Schnitzler, K.-G., Wetzel, P., and Jungclaus, J.: Will the tropical land biosphere dominate the climate-carbon cycle feedback during the twenty-first century?, Clim. Dynam., 29, 565–574, doi:10.1007/s00382-007-0247-8, 2007.

Ramaswamy, V., Boucher, O., Haigh, J., Hauglustaine, D., Haywood, J., Myhre, G., Nakajima, T., Shi, G., and Solomon, S.: Radiative Forcing of Climate Change, in: Climate Change 2001: The Scientific Basis. Contribution of working group I to the Third Assessment Report of the Intergovernmental Panel on Climate Change, edited by: Houghton, J. T., Ding, Y., Griggs, D. J., Noguer, M., van der Linden, P. J., Dai, X., Maskell, K., and Johnson, C. A., Cambridge Univ. Press, New York, 349–416, 2001.

Randall, D. A., Wood, S., Bony, R., Colman, T., Fichefet, J., Fyfe, V., Kattsov, A., Pitman, J., Shukla, J., Srinivasan, R. J., Stouffer, A., Sumi, A., and Taylor, K. E.: Climate Models and their Evaluation, in: Climate Change 2007: The Physical Science Basis. Contribution of Working Group I to the Fourth Assessment Report of the Intergovernmental Panel on Climate Change, edited by: Solomon, S., Qin, D., Manning, M., Chen, Z., Marquis, M., Averyt, K. B., Tignor, M., and Miller, H. L., Cambridge Univ. Press, New York, 589–662, 2007.

Ricke, K. L., Morgan, M. G., and Allen, M. R.: Regional climate response to solar-radiation management, Nat. Geosci., 3, 537–541, doi:10.1038/ngeo915, 2010.

Rickels, W., Klepper, G., Dovern, J., Betz, G., Brachatzek, N., Cacean, S., Güssow, K., Heintzenberg, J., Hiller, S., Hoose, C., Leisner, T., Oschlies, A., Platt, U., Proelss, A., Renn, O., Schäfer, S., and Zürn, M.: Large-Scale Intentional Interventions into the Climate System? – Assessing the Climate Engineering Debate. Scoping report conducted on behalf of the German Federal Ministry of Education and Research (BMBF), Kiel Earth Institute, Kiel, Germany, 2011.

Robock, A., Oman, L., and Stenchikov, G. L.: Regional climate responses to geoengineering with tropical and Arctic SO_2 injections, J. Geophys. Res., 113, D16101, doi:10.1029/2008JD010050, 2008.

Robock, A., Bunzl, M., Kravitz, B., and Stenchikov, G. L.: A Test for Geoengineering?, Science, 327, 530–531, doi:10.1126/science.1186237, 2010.

Seland, Ø., Iversen, T., Kirkevåg, A., and Storelvmo, T.: Aerosol-climate interactions in the CAM-Oslo atmospheric GCM and investigation of associated basic shortcomings, Tellus A, 60, 459–491, 2008.

Shepherd, J., Caldeira, K., Cox, P., Haigh, J., Keith, D., Launder, D., Mace, G., MacKerron, G., Pyle, J., Rayner, S., Redgwell, C., and Watson, A.: Geoengineering the Climate: Science, Governance and Uncertainty, The Royal Society, London, UK, 2009.

Stevens, B., Crueger, T., Esch, M., Giorgetta, M., Mauritsen, T., Rast, S., Schmidt, H., Bader, J., Block, K., Brokopf, R., Fast, I., Kinne, S., Kornblueh, L., Lohmann, U., Pincus, R., Reichler, T., Salzmann, M., and Roeckner, E.: The Atmospheric Component of the MPI-M Earth System Model: ECHAM6, J. Adv. Model. Earth Syst., submitted, 2012.

Taylor, K. E., Stouffer, R. J., and Meehl, G. A.: An Overview of CMIP5 and the experiment design, B. Am. Meteorol. Soc., 93, 485–498, doi:10.1175/BAMS-D-11-00094.1, 2012.

The HadGEM2 Development Team: Martin, G. M. Bellouin, N., Collins, W. J., Culverwell, I. D., Halloran, P. R., Hardiman, S. C., Hinton, T. J., Jones, C. D., McDonald, R. E., McLaren, A. J., O'Connor, F. M., Roberts, M. J., Rodriguez, J. M., Woodward, S., Best, M. J., Brooks, M. E., Brown, A. R., Butchart, N., Dearden, C., Derbyshire, S. H., Dharssi, I., Doutriaux-Boucher, M., Edwards, J. M., Falloon, P. D., Gedney, N., Gray, L. J., Hewitt, H. T., Hobson, M., Huddleston, M. R., Hughes, J., Ineson, S., Ingram, W. J., James, P. M., Johns, T. C., Johnson, C. E., Jones, A., Jones, C. P., Joshi, M. M., Keen, A. B., Liddicoat, S., Lock, A. P., Maidens, A. V., Manners, J. C., Milton, S. F., Rae, J. G. L., Ridley, J. K., Sellar, A., Senior, C. A., Totterdell, I. J., Verhoef, A., Vidale, P. L., and Wiltshire, A.: The HadGEM2 family of Met Office Unified Model climate configurations, Geosci. Model Dev., 4, 723–757, doi:10.5194/gmd-4-723-2011, 2011.